nature climate change

LETTERS

PUBLISHED ONLINE: 9 SEPTEMBER 2012 | DOI: 10.1038/NCLIMATE1683

# Geophysical limits to global wind power

Kate Marvel[1]*, Ben Kravitz[2] and Ken Caldeira[2]

**There is enough power in Earth's winds to be a primary source of near-zero-emission electric power as the global economy continues to grow through the twenty-first century. Historically, wind turbines are placed on Earth's surface, but high-altitude winds are usually steadier and faster than near-surface winds, resulting in higher average power densities[1]. Here, we use a climate model to estimate the amount of power that can be extracted from both surface and high-altitude winds, considering only geophysical limits. We find wind turbines placed on Earth's surface could extract kinetic energy at a rate of at least 400 TW, whereas high-altitude wind power could extract more than 1,800 TW. At these high rates of extraction, there are pronounced climatic consequences. However, we find that at the level of present global primary power demand (∼18 TW; ref. 2), uniformly distributed wind turbines are unlikely to substantially affect the Earth's climate. It is likely that wind power growth will be limited by economic or environmental factors, not global geophysical limits.**

Here, we quantify geophysical limits to wind power by applying additional drag forces that remove momentum from the atmosphere in a global climate model. We perform simulations in which drag is applied to either the near-surface environment or the entire atmosphere, and analyse consequences for the atmospheric kinetic energy budget and climate. When small amounts of additional drag are added to the atmosphere, the rate of kinetic energy extraction (KEE) increases. However, in the limit of infinite drag, the atmosphere is motionless and there is no kinetic energy to extract. This suggests that there must be some amount of added drag that maximizes KEE. We refer to this maximum KEE as the geophysical limit to global wind power. Here, we consider only geophysical limitations, not technical or economic constraints on wind power.

The large-scale climate impacts of increased surface drag have been considered in previous studies. In an idealized global climate model, surface friction was uniformly increased across the globe, and this was found to decrease atmospheric kinetic energy and shift eddy-driven mid-latitude jets polewards[3]. In a general circulation model with specified sea surface temperatures, altered surface drag and modified surface roughness height over selected regions, caused slight increases in global surface temperatures[4]. This effect was also observed when land-surface roughness was increased in a climate model incorporating a mixed-layer ocean[5]. Other studies have investigated the wind anomaly patterns produced by isolated regions of increased surface roughness[6]; and estimated wind resource potential over land that was not ice-covered[7]. However, these studies focused solely on increased surface drag. The effects of increased drag in the interior of the atmosphere have been studied[8] where a drag term was added to regions of the atmosphere where wind speeds exceeded a cutoff velocity. Unfortunately, aspects of that work make their results difficult to interpret. For example, they include wake turbulence in a term that involves momentum transfer to the turbine blades despite the fact that there is no such momentum transfer in the wake and introduce a frictional parameter with units that are difficult to reconcile with their equations.

## Results

**Limits on wind power availability.** We differentiate among three types of kinetic energy loss represented in the CAM3.5 model[9]:

- Viscous dissipation refers to the rate at which work is done by viscosity of air in converting mean and turbulent kinetic energy to internal energy through heat.
- Roughness dissipation refers to the rate at which pre-existing surface momentum sinks such as the land or ocean surface dissipate kinetic energy.
- KEE refers to the removal of kinetic energy caused by momentum loss to the added momentum sinks. In the case of wind turbines, the kinetic energy would be converted to mechanical or electrical energy, most of which would ultimately be dissipated as heat. In our simulations, this heat is dissipated locally. Drag added to the atmosphere has important secondary consequences: the velocity change and associated velocity gradients may affect both roughness and viscous dissipation. Here, KEE refers only to the rate of transfer of kinetic energy to added momentum sinks.

The parameter we introduce to vary additional drag is $\rho_{\mathrm{Area}}$: the effective extraction area per unit volume, discussed in Methods and Supplementary Section SA.1. Figure 1a shows KEE as a function of $\rho_{\mathrm{Area}}$ for cases where drag has been added to the near-surface layers (cases labelled SL($n$)) and whole atmosphere (cases labelled WA($n$)). (See also Supplementary Fig. SA.1a for the results on logarithmic scales.) As expected for low values of added drag, increasing extraction area increases KEE, that is, $(\mathrm{d(KEE)}/\mathrm{d}\rho_{\mathrm{Area}}) > 0$. At the geophysical limit to global wind power, $(\mathrm{d(KEE)}/\mathrm{d}\rho_{\mathrm{Area}}) = 0$. As shown in Fig. 1b, for both the near-surface and whole-atmosphere cases we approach but do not reach this limit. Therefore, the geophysical limits exceed the maximum KEE values found in our study for both cases.

Figure 1b shows the depletion of atmospheric kinetic energy as a function of KEE. We find that for every additional watt dissipated by drag added in the near-surface cases, total atmospheric kinetic energy decreases by 80 kJ, whereas each additional watt dissipated in the whole-atmosphere cases decreases atmospheric kinetic energy by 400 kJ.

From Fig. 1a,b we can infer that the geophysical limit on wind power availability is greater than 428 TW in the surface-only cases, and greater than 1,873 TW in the whole-atmosphere cases. These lower bounds on geophysical limits on airborne wind power exceed the present global primary energy demand of 18 TW by factors greater than 20 and 100, respectively. The results from all cases are summarized in Supplementary Table SA1.

**Kinetic energy production and the atmospheric heat engine.** In steady state, net kinetic energy dissipation is balanced by net kinetic energy production. Furthermore, in the atmosphere, kinetic energy is produced by conversion of available potential

[1]Program for Climate Model Diagnosis and Intercomparison, Lawrence Livermore National Laboratory, PO Box 808, L-103 Livermore, California 94551, USA, [2]Carnegie Institution Department of Global Ecology, 260 Panama Street, Stanford, California 94305, USA. *e-mail: marvel1@llnl.gov.

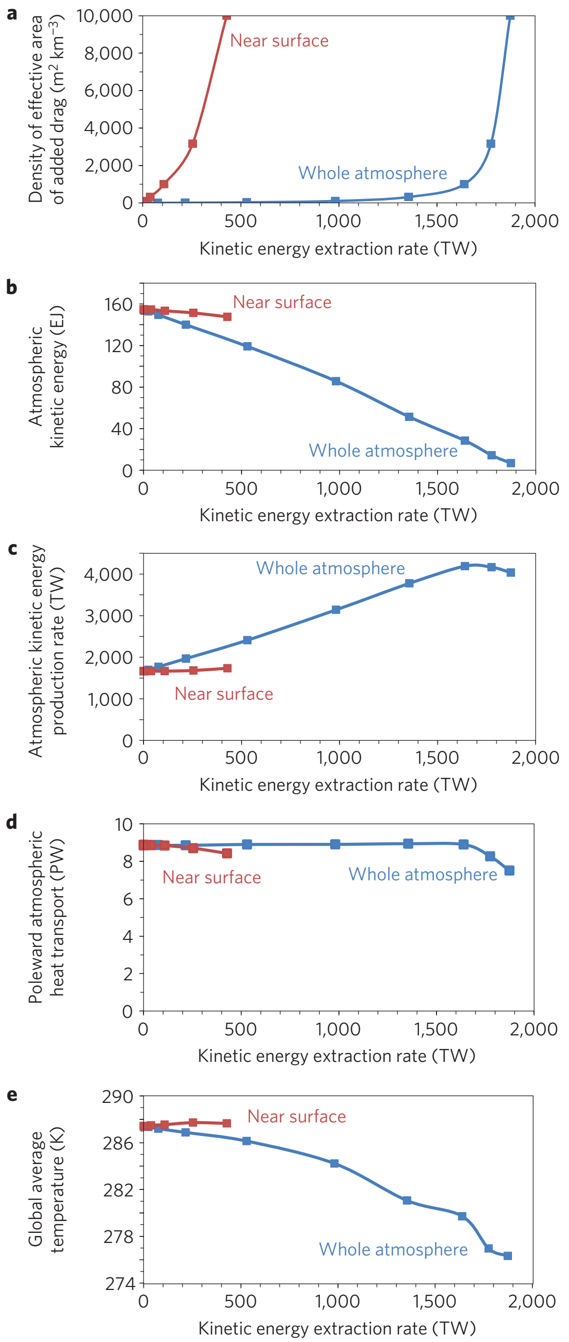


**Figure 1 | Global results for climate model simulations with drag added near the surface and throughout the whole atmosphere.** The horizontal axis for all panels is the global total amount of KEE. **a**, Areal density of effective drag added needed to produce the specified amount of global total KEE. **b**, Atmospheric kinetic energy decreases nearly linearly with KEE. **c**, The production rate of atmospheric kinetic energy is relatively insensitive to added surface drag but increases by about 0.8 W for each watt of KEE. **d**, Total poleward atmospheric heat transport is not markedly affected by added drag, except when very large amounts of drag are added to the atmosphere in the whole-atmosphere cases. **e**, Global average temperature decreases markedly in the whole-atmosphere cases.

energy. Therefore, sustained increases in net dissipation imply increases in net production of available potential energy and conversion to kinetic energy.

Figure 1c shows the total rate of dissipation (the sum of viscous dissipation, roughness dissipation and KEE) as a function of KEE.

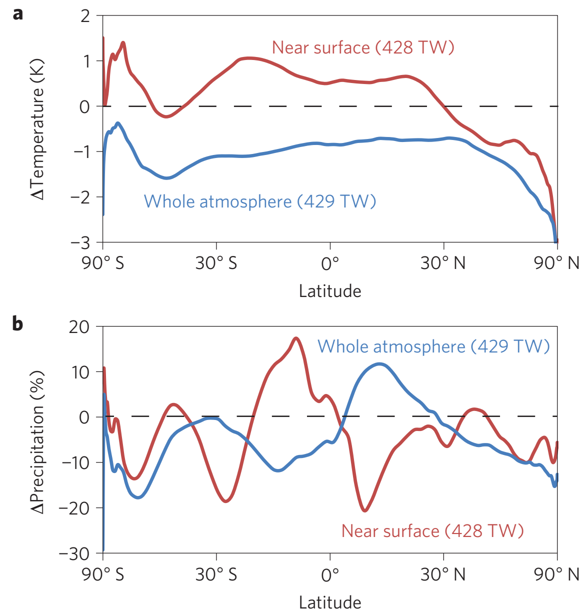


**Figure 2 | Zonal mean departures for cases extracting 428–429 TW from atmospheric winds, expressed as departures from zonal mean values in the control case.** The red lines are for the SL(5) case with an effective areal density of added drag of $10^4$ m$^2$ km$^{-3}$. The blue lines are for the WA(7.63) case with an effective areal density of added drag of 24.3 m$^2$ km$^{-3}$. **a**, Temperature departures in K. **b**, Precipitation departures as a percentage of control simulation values. These figures represent results for kinetic energy extractions levels that exceed energy demands from civilization by more than a factor of 20.

For the near-surface cases, there is little change in total atmospheric dissipation. However, in the whole-atmosphere cases, for every watt increase of KEE due to added drag cases, total atmospheric kinetic energy production increases by ~0.8 W. The near-linear relationship between added dissipation and total dissipation holds until the KEE in the whole atmosphere exceeds ~1,600 TW. Beyond this value, increases in KEE result in declines in net kinetic energy production.

Figure 1d depicts the net atmospheric energy transport from low latitudes with net atmospheric energy gain to high latitudes with net atmospheric energy loss. To a large extent, atmospheric energy transports must adjust such that energy is transported in steady-state from regions of net energy accumulation to regions of net energy loss. When drag is added near the surface alone, high KEE does cause some decrease in net poleward energy transport. For the whole-atmosphere cases, however, net energy transport remains approximately constant until KEE exceeds ~1,600 TW, after which it declines sharply.

**Climate impacts.** Figure 1e indicates that uniformly applied surface drag has a slight warming effect, consistent with previous studies[4,5,10]. However, we find that whole-atmosphere drag can have a large surface cooling effect as KEE approaches the geophysical limit. If we assume that the effects of extracting kinetic energy scale linearly at extraction rates less than 429 TW, then satisfying global energy demand with uniformly distributed wind turbines would cause a global mean temperature increase of 0.03 K for near-surface wind turbines, and a global mean decrease of 0.007 K for turbines distributed throughout the atmosphere.

Figure 2 shows zonal mean temperature change and percentage change in zonal mean precipitation for cases SL(5) and WA(7.63), each of which have approximately the same globally integrated KEE (428 TW and 429 TW, respectively). Zonal mean temperature

 DOI: 10.1038/NCLIMATE1683 

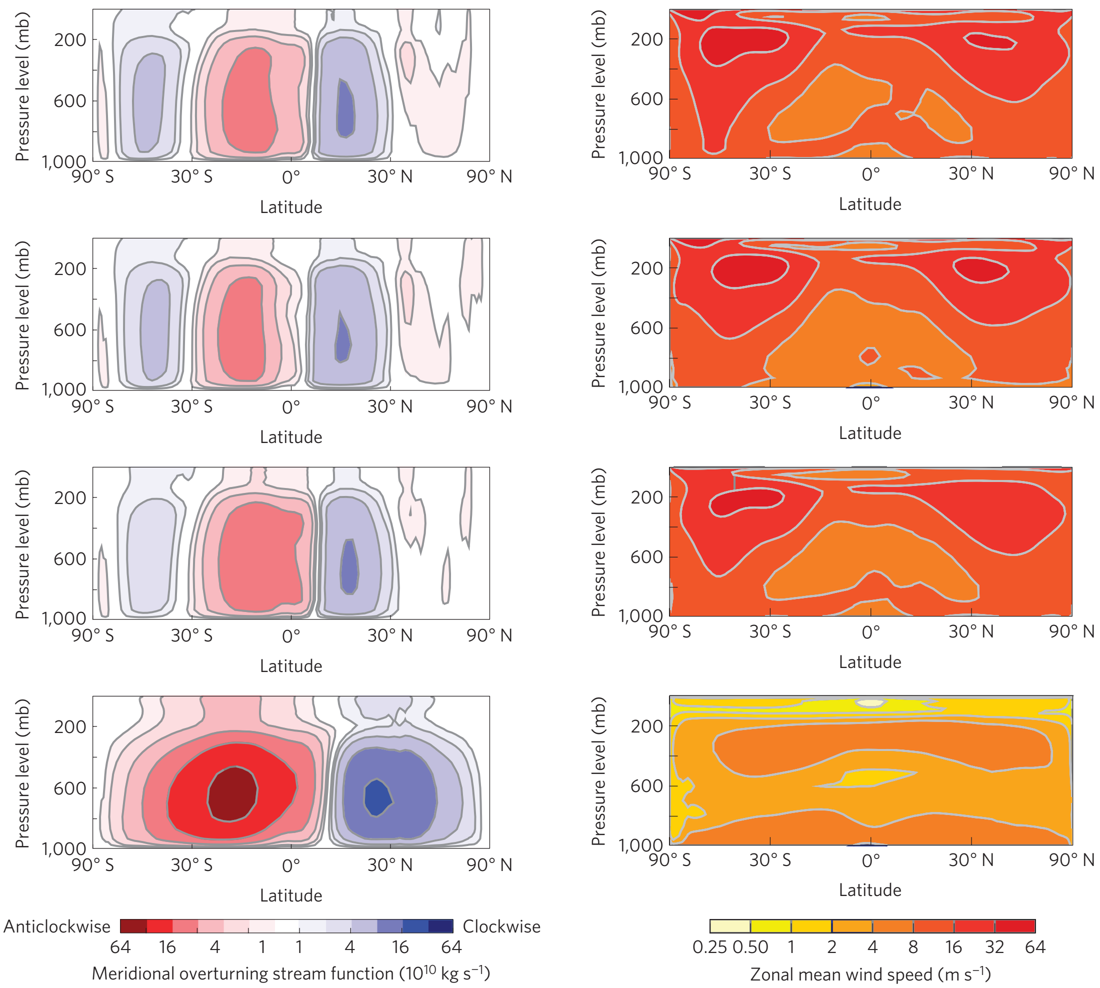


**Figure 3 | Circulation changes from large-scale kinetic energy extraction.** The left column shows the meridional mass overturning stream function, in $10^{10}$ kg m s$^{-1}$ for (from top to bottom) the selected cases, control, SL(5), WA(7.63) and WA(5). Cases SL(5) and WA(5) were chosen because they are our lower-bound estimates of near-surface and whole-atmosphere maximum KEE rates at 428 TW and 1,873 TW, respectively. WA(7.63) was chosen as a whole-atmosphere case that has a similar KEE (429 TW) to the SL(5) case. The right column shows zonal mean wind speeds for (from top to bottom) the control, SL(5), WA(7.63) and WA(5). Cases SL(5) and WA(5) have added drag with areal density $10^4$ m$^2$ km$^{-3}$ in the near-surface and whole atmosphere, respectively. Case WA(7.63) has added drag with areal density 24.3 m$^2$ km$^{-3}$ in the whole atmosphere.

changes in these cases are of the order of 1 K and percentage changes in zonal mean precipitation are of the order of 10%. This suggests that, at the scale of global energy demand, uniformly distributed wind power would produce zonal mean temperature changes of ~0.1 K and changes in zonal mean precipitation of ~1% (see Supplementary Section SA2). Thus, reliance on widely distributed wind turbines as an energy source is unlikely to have a substantial climate impact.

**Circulation changes.** Many quantities shown in Fig. 1 scale nearly linearly with KEE at rates less than ~1,600 TW. Our results suggest that the breakdown of this linear relationship above ~1,600 TW is due to a regime shift in the atmospheric circulation. Figure 3 shows the meridional overturning stream function for four cases: the control run, SL(5), WA(7.63) and WA(5). SL(5) and WA(5) are chosen because they represent the maximum simulated KEE for near-surface-alone and whole-atmosphere drag, respectively. The meridional overturning stream function for the SL(5) seems similar to that of the control simulation. The stream function for WA(7.63) is less similar, despite the similar amount of KEE. In particular, the downward branches of the Hadley cells shift polewards. In the extreme case of WA(5) the Hadley cells extend to the poles, and poleward heat transport is carried out in each hemisphere by a single large cell. As discussed in Supplementary Section SA3, similar effects have been observed in numerical and laboratory experiments in which the viscosity of the atmosphere is increased or the Earth's rotation rate is decreased[11–14].

The right-hand column of Fig. 3 shows zonal mean wind speed as a function of latitude and pressure. The control case has global mass-weighted average wind speeds of 18.5 m s$^{-1}$ and pronounced mid-latitude jets at around 200 mb. SL(5) shows a similar pattern, with global average wind speeds of 17.9 m s$^{-1}$, but near-surface winds are reduced by ~30% (see Fig. 1h). Mean wind speeds in WA(7.63) are 15.7 m s$^{-1}$, and the upper level jets weaken, particularly in the Northern Hemisphere. In the extreme whole-atmosphere case WA(5), mean wind speeds decrease precipitously to 3.1 m s$^{-1}$.

## Discussion and conclusions

In this study, we establish lower bounds on the maximum rate at which kinetic energy may be extracted from the atmosphere by added momentum sinks. Using a climate model, we simulate this extraction by adding drag to the near-surface layers alone, and to the WA($n$). We find that when drag is added uniformly to the near-surface environment, it is possible to extract kinetic energy at rates exceeding 428 TW, whereas when drag is added uniformly throughout the entire atmosphere the lower bound exceeds 1,873 TW. The present total global power demand is ~18 TW (ref. 2).

We find that civilization-scale reliance on wind power, if uniformly distributed, might change zonal mean temperature by ~0.1 K and zonal mean precipitation by ~1%. Consistent with previous literature, we find that large-scale near-surface KEE has a small surface warming effect, whereas whole-atmosphere KEE has a cooling effect. In both cases we observe a decrease in global average precipitation.

If the Earth were not rotating, atmospheric mass would accelerate down pressure gradients, rapidly converting available potential energy to kinetic energy. In contrast, on a rotating Earth with an atmosphere with zero viscosity, apparent Coriolis forces would balance pressure gradient forces and flows would be geostrophic (that is, along surfaces of constant pressure), with no conversion of potential to kinetic energy. Added drag forces cause atmospheric flows to depart further from geostrophy, and thus permit more rapid conversion of available potential energy to kinetic energy (see Supplementary Information). Increased net kinetic energy production can be sustained only by increased net production of available potential energy (APE). Increased production of APE results from increased diabatic heating of warm air masses or decreased diabatic heating of cool air masses. In our simulations, the area of snow- and ice-covered land expands as KEE increases. One source of increased production of APE in these simulations is the decreased diabatic heating over these newly snow- and ice-covered regions.

To obtain limits on the rate at which kinetic energy may be extracted from the atmosphere, we consider only the idealized cases in which drag is uniformly applied. We show that roughly equivalent amounts of KEE have different consequences for the Earth's climate and general circulation, depending on whether the extraction is confined to the near-surface or is applied throughout the whole atmosphere. This strongly suggests that our results would be different had we restricted this drag by applying it to high-velocity winds, to certain geographical regions or to specified vertical levels. Future work will investigate these cases, and will establish geophysical limits on wind power extraction in more realistic contexts. However, it seems that the future of wind energy will be determined by economic, political and technical constraints, rather than global geophysical limits.

## Methods

All simulations were performed using the National Center for Atmospheric Research Community Atmosphere Model, Version 3.5 (CAM3.5) in a configuration with a mixed-layer ocean with specified ocean heat transport[15]. The model resolution was 2° in latitude by 2.5° in longitude with 26 levels in the vertical dimension. All simulations were integrated for 100 years. Simulations approach a stationary state on the timescale of decades; the final 60 years of each simulation were used for analysis.

A series of simulations (labelled SL($n$)) were performed with drag added to the two lowest model layers, schematically representing ground-based wind turbines, with effective extraction areas per unit volume of atmosphere of $\rho_{\mathrm{Area}} = 10^{-n}\,\mathrm{m}^{-1}$ for $n = \{5, 5.5, \ldots 8.5, 9\}$. Another series of simulations (labelled WA($n$)) had drag forces applied throughout the whole atmosphere using the same values of $\rho_{\mathrm{Area}}$. Note that these simulations correspond to effective drag areas ranging from one square metre per cubic kilometre of model atmosphere (the $n = 9$ cases) to 10,000 $\mathrm{m}^2\,\mathrm{km}^{-3}$ ($n = 5$). Two further simulations were performed: a control run with $\rho_{\mathrm{Area}} = 0$, and a simulation labelled WA(7.63) with effective drag area 23.4 $\mathrm{m}^2\,\mathrm{km}^{-3}$, designed to yield a global average KEE rate similar to the SL(5) case.

Received 1 May 2012; accepted 8 August 2012; published online 9 September 2012

## References


1. Archer, C. & Caldeira, K. Global assessment of high-altitude wind power. *Energies* **2,** 307–319 (2009).
2. US Energy Information Administration. International energy statistics database. Accessed May 2012; available at www.eia.gov/ies.
3. Chen, G., Held, I. & Robinson, W. Sensitivity of the latitude of the surface westerlies to surface friction. *J. Atmos. Sci.* **64,** 2899–2915 (2007).
4. Keith, D. W. *et al.* The influence of large-scale wind power on global climate. *Proc. Natl Acad. Sci. USA* **101,** 16115–16120 (2004).
5. Wang, C. & Prinn, R. Potential climatic impacts and reliability of very large-scale wind farms. *Atmos. Chem. Phys.* **10,** 2053–2061 (2010).
6. Kirk-Davidoff, D. & Keith, D. On the climate impact of surface roughness anomalies. *J. Atmos. Sci.* **65,** 2215–2234 (2008).
7. Miller, L. M., Gans, F. & Kleidon, A. Estimating maximum global land surface wind power extractability and associated climatic consequences. *Earth Syst. Dynam.* **2,** 1–12 (2011).
8. Miller, L., Gans, F. & Kleidon, A. Jet stream wind power as a renewable energy resource: Little power, big impacts. *Earth Syst. Dynam.* **2,** 201–212 (2011).
9. Boville, B. & Bretherton, C. Heating and kinetic energy dissipation in the NCAR community atmosphere model. *J. Clim.* **16,** 3877–3887 (2003).
10. Zhou, L. *et al.* Impacts of wind farms on land surface temperature. *Nature Clim. Change* **2,** 539–543 (2012).
11. Hide, R. An experimental study of thermal convection in a rotating liquid. *Phil. Trans. R. Soc. Lond. A* **250,** 441–478 (1958).
12. Del Genio, A. & Suozzo, R. A comparative study of rapidly and slowly rotating dynamical regimes in a terrestrial general circulation model. *J. Atmos. Sci.* **44,** 973–986 (1987).
13. Navarra, A. & Boccaletti, G. Numerical general circulation experiments of sensitivity to earth rotation rate. *Clim. Dynam.* **19,** 467–483 (2002).
14. Hunt, B. The influence of the earth's rotation rate on the general circulation of the atmosphere. *J. Atmos. Sci.* **36,** 1392–1408 (1979).
15. Collins, W. *et al.* *Description of the NCAR Community Atmosphere Model (CAM 3.0)* Technical Report, (National Center for Atmospheric Research, 2004).



## Acknowledgements

We wish to thank L. Cao for his help in configuring and running CAM and C. Doutriaux, P. Caldwell and K. Taylor for useful discussions. This work was performed under the auspices of the US Department of Energy by Lawrence Livermore National Laboratory under Contract DE-AC52-07NA27344.


## Author contributions

K.M. and K.C. designed the study. K.M. prepared and performed the simulations. K.M., K.C. and B.K. analysed the data. K.M. and K.C. wrote the paper with contributions from B.K.

## Additional information

Supplementary information is available in the online version of the paper. Reprints and permissions information is available online at www.nature.com/reprints. Correspondence and requests for materials should be addressed to K.M.

## Competing financial interests

The authors declare no competing financial interests.

nature climate change

SUPPLEMENTARY INFORMATION
DOI: 10.1038/NCLIMATE1683

# Geophysical limits to global wind power

Kate Marvel
Program for Climate Model Diagnosis and Intercomparison
Lawrence Livermore National Laboratory
P.O. Box 808, L-103
Livermore, CA 94551 USA
marvel1@llnl.gov

Ben Kravitz
Carnegie Institution
Department of Global Ecology
260 Panama Street
Stanford, CA 94305 USA
bkravitz@dge.stanford.edu

Ken Caldeira
Carnegie Institution
Department of Global Ecology
260 Panama Street
Stanford, CA 94305 USA
kcaldeira@dge.stanford.edu

August 17, 2012

# A Supporting Online Material

## A.1 Drag Parametrization

In this section, we discuss the parameter $\rho_{Area}$ used to represent the large-scale effects of additional momentum sinks. This parameter, which has units of inverse length, represents the effective area covered by drag per square meter of atmosphere. $\rho_{Area} = 10^{-9}$ therefore corresponds to one square meter of extraction area per cubic kilometer of atmosphere, while the largest value used here, $\rho_{Area} = 10^{-5}$, corresponds to 10,000 square meters of extraction area per cubic kilometer. An increase in $\rho_{Area}$ therefore corresponds to an increase in effective drag. Alternatively, this term can be thought of as the inverse of a kinetic energy extraction length scale $L$: the mean distance a parcel of air moves before losing its momentum to added momentum sinks (i.e., additional drag). Thus, when $\rho_{Area} = 10^{-9}$, the average parcel of air travels one million kilometers before losing its momentum to the additional sinks, and when $\rho_{Area} = 10^{-5}$, a parcel of air may travel only 100 km before losing momentum.

This means that the effect of additional drag may also be parameterized in terms of a timescale for kinetic energy extraction. This is, equivalently, the timescale for energy to be transported to effective drag areas. This time scale varies in space and time and is inversely proportional to local wind speed. Figure A1(d) shows the quotient of the global total kinetic energy extraction rate and the global total atmospheric kinetic energy for each of our simulations. In the SL simulations, this timescale ranges from almost 200 years in the SL(9) case to 20 days in the SL(5) cases. In the WA simulations, the timescale ranges from one year to about 5 hours. Figure A1(e), by contrast, show the kinetic energy *residence* time, defined as the quotient of the total dissipation rate and the total kinetic energy.

These momentum sinks reduce the kinetic energy of the atmosphere through two basic mechanisms. First, as momentum is transferred by the added drag (to, e.g., a turbine blade), the winds slow. Second, this change in mean-flow wind speed will create horizontal and vertical gradients in wind speed, resulting in increased turbulent transfer of momentum. As momentum is transferred from air parcels with high wind speed to air parcels with lower speed, overall kinetic energy is reduced, with the deficit dissipated as heat.

$\rho_{Area}$ can be related to the more familiar drag coefficient. Consider air

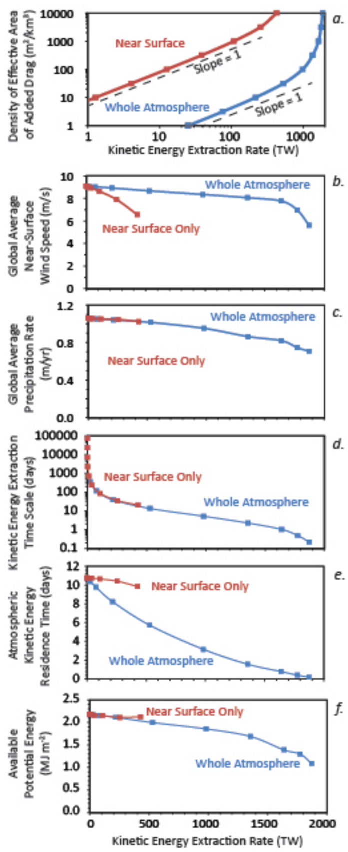


Figure A.1: Selected quantities as a function of KEE for near-surface and whole-atmosphere drag. (a) Log plot of $\rho_{Area}$. (b) Global average near-surface wind speed. (c) Global mean precipitation rate. (d) Kinetic energy extraction time scale. (e) Kinetic energy residence time.

with velocity $\mathbf{v}$ incident on a disk with area $\mathbf{A} = A\hat{n}$ oriented in the $\hat{n}$ direction. Let the velocity at the disk be $\mathbf{v_D}$ and the velocity in the far wake $\mathbf{v_W}$. The mass flow through the disk is therefore

$$\dot{m} = \rho \mathbf{A} \cdot \mathbf{v_D}. \tag{1}$$

Momentum is transferred to the disk by the incident air, so the disk exerts a net force

$$\mathbf{F} = m\frac{d\mathbf{v}}{dt} = \dot{m}\Delta v = -(\rho \mathbf{A} \cdot \mathbf{v_D})(\mathbf{v} - \mathbf{v_W}) \tag{2}$$

on the moving air. The rate at which the wind does work on the disk is:

$$P = -\mathbf{F} \cdot \mathbf{v_D} = \rho \mathbf{A} \cdot (\mathbf{v} - \mathbf{v_W})|\mathbf{v_D}|^2. \tag{3}$$

(Note the negative sign enters because the force is defined as the force exerted by the disk on the air, but power is defined as work done by air on the disk). Alternately, by conservation of energy, the power can be calculated as the difference between the power in the wind at the front of the disk and the power in the far wake:

$$P = \frac{1}{2}\rho \mathbf{A} \cdot \mathbf{v_D}(\mathbf{v}^2 - \mathbf{v_W}^2). \tag{4}$$

Equating (3) and (4) we find

$$\mathbf{v_D} = \frac{1}{2}(\mathbf{v} + \mathbf{v_W}). \tag{5}$$

Define $b = \frac{|\mathbf{v_W}|}{|\mathbf{v}|}$ to be the drop in wind speed across the disk. Using (5), we can now write the power as

$$P = \left[\frac{1}{2}(1+b)^2(1-b)\right] P_0 \equiv \beta P_0 \tag{6}$$

where $P_0 = \frac{1}{2}\rho|\mathbf{A}|\cos\theta \mathbf{v_D}^3$ and $\theta$ is the angle between $\hat{n}$ and $\mathbf{v}$. This is maximized at the Betz limit when $b = \frac{1}{3}$ and the power coefficient $\beta = \frac{16}{27}$.

If we define the effective kinetic energy extraction area

$$A_{eff} = \beta|\mathbf{A}|\cos\theta \tag{7}$$

the axial force becomes

$$\mathbf{F} = -\frac{A_{eff}}{(1+b)}\rho v \mathbf{v} \tag{8}$$

"Surface" drag is often defined in terms of components of the Reynolds stress tensor $\tau$ using the dimensionless drag coefficient $C_D$:

$$\begin{aligned} \tau_{z\rho_{Area}} &= -\rho C_D |\mathbf{v}| u \\ \tau_{z\phi} &= -\rho C_D |\mathbf{v}| v \end{aligned} \tag{9}$$

The sum of these terms yields the total force per horizontal area $A_Z = V/\Delta z$ where $V$ is the unit atmospheric volume and $\Delta z$ the vertical layer thickness. Multiplying (9) through by $A_Z$ and equating with (8), we find that the drag coefficient is

$$C_D = \frac{A_{eff}}{V(1+b)} \Delta z = \rho_{Area} \Delta z (1+b)^{-1}. \tag{10}$$

Our parameter $\rho_{Area}$ is therefore proportional to the drag coefficient divided by the layer thickness.

## A.2 Spatial distribution of kinetic energy extraction

Figure A.2 shows the vertically integrated kinetic energy extraction rate KEE for three wind energy extraction cases. For the extreme near-surface case SL(5) ($\rho_{Area} = 10^{-5}\mathrm{m}^{-1}$ in the model's lowest two layers), 428 TW is extracted. The highest values of KEE are over ocean area and exceed 2 W $\mathrm{m}^{-2}$. In the analogous whole-atmosphere case WA(7.63) ($\rho_{Area} = 10^{-7.63}\mathrm{m}^{-1}$ throughout the entire model atmosphere), 429 TW is extracted. KEE reaches maximum values exceeding 2 W m-2 between 20° and 40° latitude in both hemispheres. Finally, in the extreme whole-atmosphere case WA(5) ($\rho_{Area} = 10^{-5}$ $\mathrm{m}^{-1}$ throughout the entire model atmosphere), 1827 TW is extracted, with the highest values exceeding 8 W $\mathrm{m}^{-2}$ in a few isolated areas and exceeding 4 W $\mathrm{m}^{-2}$ over broad regions in the mid-latitudes. While the amount of KEE is similar in the SL(5) and WA(7.63) cases, the regions of maximum extraction in SL(5) are associated with strong mid-latitude surface winds, whereas the regions of maximum extraction in the WA(7.63) cases are associated with the jet streams. In the WA(5) case, the jets have been largely suppressed, and energy extraction is distributed over a broader geographic region.

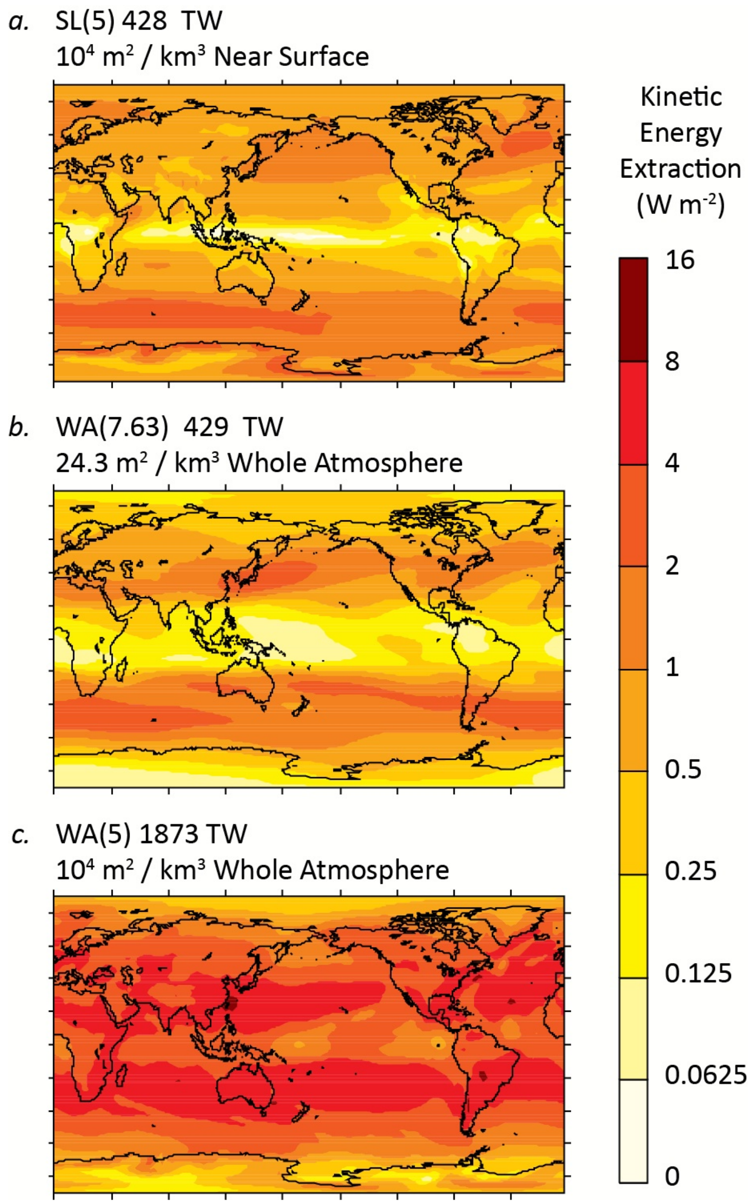


Figure A.2: Vertical integral of kinetic energy extraction (KEE) from climate model simulations with drag added near the surface and throughout the whole atmosphere: (a) SL(5), (b) WA(7.63), (c) WA(5).

## A.3 Angular Momentum Constraints and the General Circulation

One major consequence of increased whole-atmosphere drag is an extension of the atmospheric Hadley regime into higher latitudes. This effect is most pronounced in the cases with the greatest amounts of added drag. In the cases with the greatest amount of added drag, there is a regime shift in atmospheric circulation characterized by Hadley cells that extend from the equator to the poles. Many global mean properties scale approximately linearly with KEE, but this scaling breaks down when the atmospheric circulation undergoes this regime shift (see Figure 1 in the main text).

The mechanisms underlying this regime shift can be illustrated by considering a ring of air above the equator that rises and begins to move poleward in an atmosphere with neither friction nor drag. Consider an azimuthally symmetric ring of air located at the equator with initial zonal velocity $u = 0$. In the absence of torques due to frictional forces or added drag, angular momentum is conserved as the ring rises and moves poleward. We therefore have

$$\frac{d}{dt}\left[ua\cos(\theta) + \Omega a^2\cos^2(\theta)\right] = 0 \tag{11}$$

where $a$ is the radius of the Earth. As the latitude $\theta$ approaches $\pm 90°$, the zonal velocity must increase so that at latitude $\theta_1$

$$u(\theta_1) = \Omega a \tan(\theta_1)\cos(\theta_1).$$

This expression is singular at the poles, meaning that on a rotating sphere an axisymmetric ring of air moving poleward must acquire infinite angular momentum. In practice, the development of baroclinic eddies in the mid-latitudes breaks axial symmetry, leading to the development of a pressure gradient torque which appears on the right-hand side of Eq. 11 and constrains the increase of atmospheric angular momentum.

The drag force acts opposite to the prevailing wind direction with a magnitude given by (2). This means that the conservation equation is modified:

$$\frac{d}{dt}\left[ua\cos(\theta) + \Omega a^2\cos^2(\theta)\right] = \left(-\rho_{Area}\frac{|\mathbf{v}|u}{(1+b)} + F_{\rho_{Area}}\right) a\cos\theta \tag{12}$$

where $F_{\rho_{Area}}$ is the contribution from frictional and pressure forces. If we neglect this final term, an increase in zonal velocity $u$ also leads to an increase in angular momentum loss due to added drag. In extreme cases, this means that the change in angular momentum of an axisymmetric ring may be very large, and the conditions that force the breaking of this symmetry may not appear; that is, direct meridional transport may become possible.

To illustrate this shift in the atmospheric circulation, we consider the meridional transport of sensible heat and momentum in the four cases discussed in the main text: the control, SL(5), WA(7.63), and WA(5). Figures A.3 and A.4 show the meridional transport of sensible heat and momentum, respectively. Figure X shows the sensible heat and momentum transport separated into mean flow and eddy contributions. In the extreme WA(5) case, eddy transport is suppressed nearly completely.

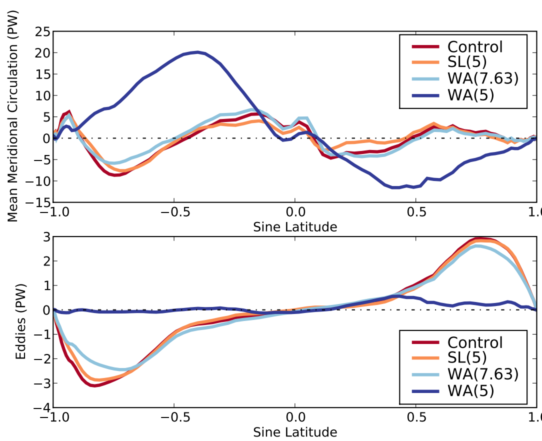


Figure A.3: Zonally and vertically averaged mean meridional (top) and transient plus stationary eddy (bottom) contributions to the meridional transport of sensible heat, in PW.

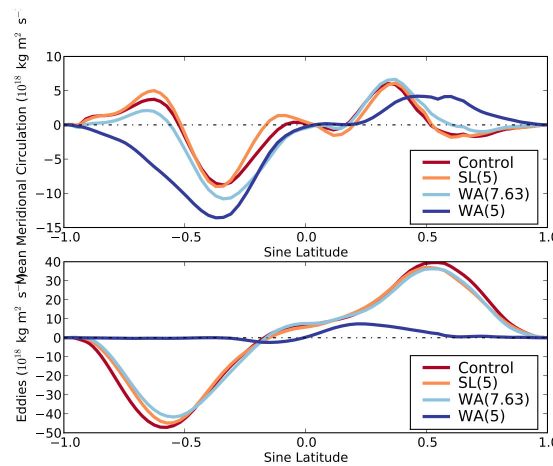


Figure A.4: Zonally and vertically averaged mean meridional (top) and transient plus stationary eddy (bottom) contributions to the meridional transport of momentum, in $10^{18}$ kg $m^2 s^{-1}$.

Rotating annulus experiments [1] confirm that the transition to eddy-dominated regimes in an idealized case is governed by the relative strength of the Coriolis forces relative to fluid viscosity. Subsequent numerical experiments [2, 3, 4] have been performed to investigate the influence of the rotation rate on the general circulation. These studies have shown that a change in the primary mode of meridional heat transport is associated with changes in tropospheric jet velocities and the efficiency with which the atmospheric heat engine converts absorbed solar radiation to kinetic energy. They indicate that decreasing the Earth's rotation period can lead to the disappearance of the mid-latitude Ferrel cell associated with baroclinic eddy activity, and in fact the results shown in Figures A.3 and A.4 are similar to those obtained by [3]. In experiments where there is substantial baroclinic activity, the rate of kinetic energy production is found to increase with decreased rotation rate due to the increasingly organized flow. Farrell [5] discusses a case in which an increase in the scale height of atmospheric circulation can bring about a single cell circulation leading to a decreased equator-to-pole temperature gradient. This temperature gradient reduction also occurs in experiments in which the Earth's rotation rate is slowed [3]. Our experiment differs from these studies in that we have neither increased the viscosity of the atmosphere nor altered the Earth's rotation rate, but incorporated additional momentum sinks into the whole atmosphere. However, an understanding of the behavior of the slowly rotating or viscous atmosphere can provide insight into our results. .

## A.4 Energetics

The atmospheric kinetic energy cycle can be simply represented by
$G \rightarrow \boxed{\mathrm{A}} \rightarrow C \rightarrow \boxed{\mathrm{K}} \rightarrow D$
where $G$ is the net generation rate of available potential energy, $A$ the available potential energy reservoir, $C$ the conversion rate between available potential and kinetic energy, and $D$ the dissipation rate. Because we our analyzed simulation period of 60 years is long relative to the residence time of kinetic energy in the atmosphere (see Figure A1(e)), we can make the assumption that the atmosphere is in steady state, and thus $G = C = D$.

Figure 1b in the main text shows how the kinetic energy reservoir $\boxed{\mathrm{K}}$ changes with increasing kinetic energy extraction. In order to calculate how the reservoir $\boxed{\mathrm{A}}$ is affected by kinetic energy extraction, we use the approximation [6]

$$\bar{A} = \frac{1}{2}\int_0^{p_0} \frac{1}{\bar{\bar{T}}} \frac{\overline{\mathrm{var(T)}}}{(\Gamma_d - \Gamma)}\, dp$$

where $\Gamma_d$ is the dry adiabatic lapse rate, $\Gamma$ the lapse rate, the temperature variance is calculated on pressure surfaces, and other notation is standard. This quantity is shown in Figure A1(f).

Evidently, large-scale kinetic energy extraction from the entire atmosphere depletes the reservoirs of available potential energy and kinetic energy. Kinetic energy is reduced because added drag slows global average wind speeds, whereas available potential energy is reduced in large part because the temperature gradient becomes weaker, reducing the temperature variance on constant-pressure surfaces. Figure A.5 shows this variance as a function of model level for both the near-surface and whole atmosphere runs.

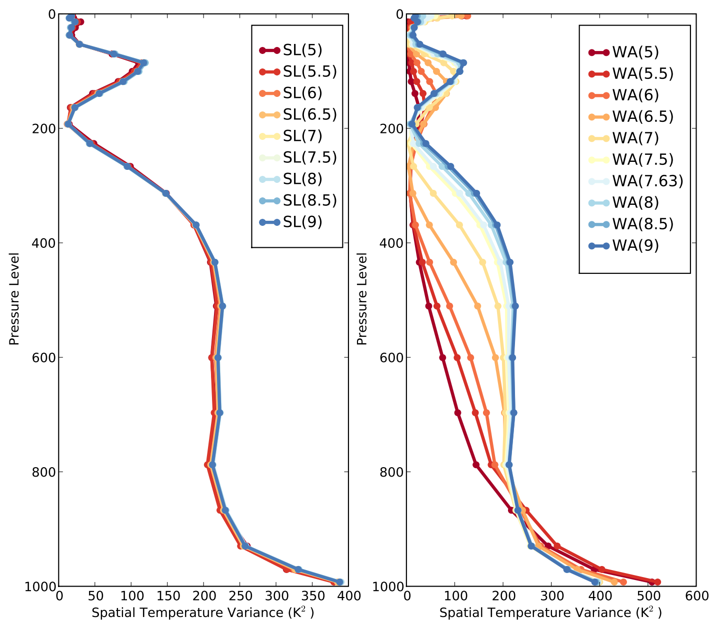


Figure A.5: Spatial variance of temperature on constant pressure surfaces as a function of height for near-surface model runs (left) and whole-atmosphere runs (right). The units are Kelvin squared.

While we assume the rate of conversion $C$ is equal to the rate of dissipation $D$ when integrated over the whole atmosphere, locally there may be a very large imbalance between these terms. For example, in the control case, there are large vertical motions in the mid-troposphere but most kinetic energy is dissipated at the surface or in the jet streams. We therefore consider the mechanical work done by a pressure layer on the atmosphere above it; this is the product of the pressure vertical velocity and the geopotential divided by the gravitational acceleration. A positive(negative) work term at a constant-pressure layer indicates work done by(on) the layer on(by) the layers above. Figure A.6 shows this work term as a function of height for the control case and for SL5, WA7.63, and WA5.

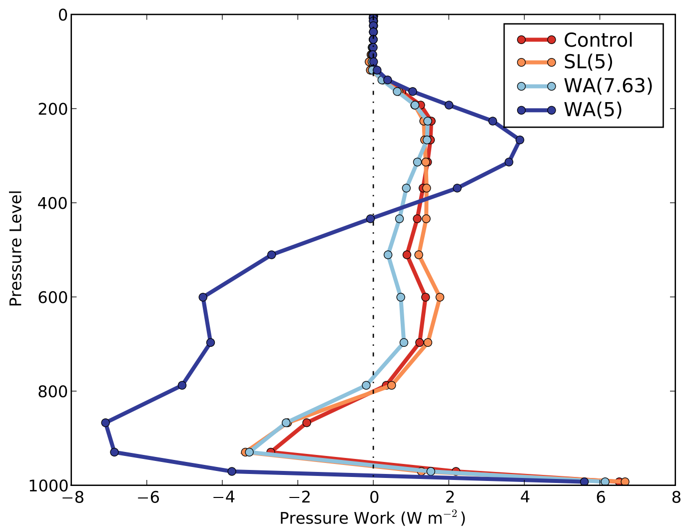


Figure A.6: Rate of pressure work done by each pressure level on the atmosphere above.

In the extreme SL(5) case, the work term becomes more negative at thse planetary boundary layer, indicating an increase in the rate of export of energy from the troposphere to the planetary boundary layer. The term becomes more positive in the mid-troposphere, indicating that the rate at which work is done by the troposphere on the stratosphere is increasing. In the WA(7.63) case, which has an amount of kinetic energy extraction similar to the SL(5) case but extracted throughout the whole atmosphere, there is likewise an increase in the downward export of energy into the boundary layer. There is also a smaller increase in the rate of upward export of energy into the stratosphere. In the extreme WA(5) case, in which direct poleward transport is the dominant transfer mechanism, we see large increases in both the downward transfer rate into the planetary boundary layer and the rate of upward transfer into the stratosphere relative to the control.

## A.5 Further notes on temperature and precipitation

Introducing near-surface drag tends to increase vertical transport, enhancing turbulent transfer of heat away from the surface, an effect observed in the field [7]. However, drag forces also reduce wind speeds, tending to suppress turbulent transport. Increased vertical transport will act to cool the surface, while a reduction in wind speeds will lead to a warming effect. Figure A1(b) shows that near-surface wind speeds drop more sharply for the SL cases than for the WA cases- an unsurprising result, since the kinetic energy extraction in the SL cases takes place only near the surface. This means that the the reduction in near-surface wind speeds dominates for near-surface extraction and we therefore expect warming, while for whole-atmosphere extraction the enhanced turbulent transport is likely responsible for the surface cooling.

Ref 6 in the main text shows a nighttime temperature increase associated with high concentrations of surface-based wind turbines. Our study pertains not to high concentrations of wind turbines, but rather to uniformly distributed wind turbines. We find little cause for concern from the climate impacts of broadly distributed wind turbines at scales that could conceivably be implemented this century. However, there is a potential regional climate concern from high local or regional densities of wind turbines.

A previous study [8] considers wind power over unglaciated land only. Their measured dissipation changes by approximately a factor of two when they change model resolution, so their results may be considered an order-of-magnitude estimate. They show about 58 TW of kinetic energy dissipation over land in their most extreme case. This compares with 90 TW dissipated over land in our most extreme near-surface wind turbine case; results from all cases are summarized in Table A1 in the supplementary material.

It is useful to separate total precipitation into large-scale and convective components, and to examine the variation of these zonally averaged quantities with latitude, as in Figure A.7. Panel (a) in Figure A7 represents zonally averaged convective as a function of latitude for four cases. In the extreme surface-only case SL(5), convective precipitation decreases slightly in the Northern Hemisphere and increases slightly in the Southern. This result is consistent with precipitation changes reported by Wang and Prinn [9], who observed a shift in the location of the Hadley circulation as a result of large-scale near-surface wind extraction. The whole-atmosphere case with equivalent kinetic energy extraction, WA(7.63), appears more similar to the control, but convective precipitation is suppressed in the Southern

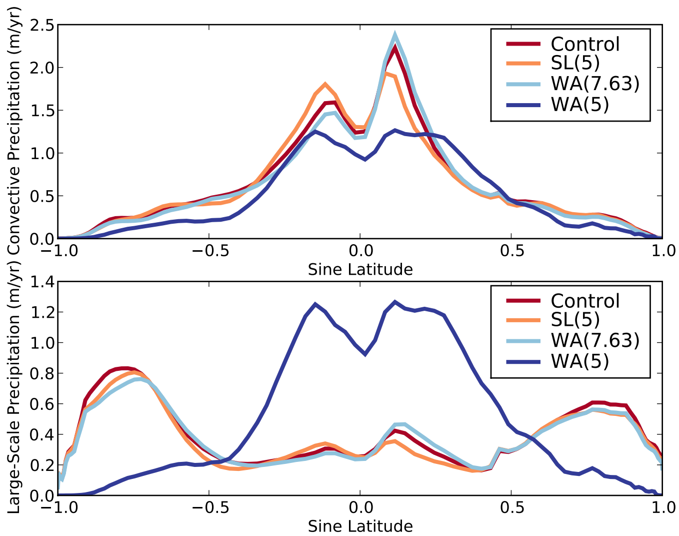


Figure A.7: Zonally averaged convective and large-scale precipitation for selected surface-only and whole-atmosphere cases.

Hemisphere and enhanced in the Northern. The extreme whole-atmosphere case WA(5)shows reduction in precipitation throughout the tropics.

Panel (b) in Figure A.7 shows zonally averaged large-scale precipitation as a function of latitude. The figure shows a decrease in mid-latitude large-scale precipitation and an increase in tropical large-scale precipitation in the WA(5) case, indicating that the mid-latitude weather systems are extremely affected by whole-atmosphere drag. The large reduction in large-scale precipitation observed in Figure A.7 is likely due to the weakening and eventual suppression of baroclinic eddy transport.

# References

[1] Hide, R. An experimental study of thermal convection in a rotating liquid. *Philosophical Transactions of the Royal Society of London. Series A, Mathematical and Physical Sciences* **250**(983), 441–478 (1958).

[2] Del Genio, A. and Suozzo, R. A comparative study of rapidly and slowly rotating dynamical regimes in a terrestrial general circulation model.

*Journal of Atmospheric Sciences* **44**, 973–986 (1987).

[3] Navarra, A. and Boccaletti, G. Numerical general circulation experiments of sensitivity to earth rotation rate. *Climate dynamics* **19**(5), 467–483 (2002).

[4] Hunt, B. The influence of the earth's rotation rate on the general circulation of the atmosphere. *Journal of Atmospheric Sciences* **36**, 1392–1408 (1979).

[5] Farrell, B. Equable climate dynamics *Journal of Atmospheric Sciences* **47**, 2986 (1990).

[6] Peixoto, J. and Oort, A. *Physics of Climate.* American Institute of PhysicsNew York (1992).

[7] Roy, S. and Traiteur, J. Impacts of wind farms on surface air temperatures. *Proceedings of the National Academy of Sciences* **107**(42), 17899–17904 (2010).

[8] Miller, L. M., Gans, F., and Kleidon, A. Estimating maximum global land surface wind power extractability and associated climatic consequences *Earth System Dynamics* **2**(1), 1-12 (2011).

[9] Wang, C. and Prinn, R. Potential climatic impacts and reliability of very large-scale wind farms. *Atmos. Chem. Phys* **10**, 2053–2061 (2010).

# List of Figures

A.1 Selected quantities as a function of KEE for near-surface and whole-atmosphere drag. (a) Log plot of $\rho_{Area}$. (b) Global average near-surface wind speed. (c) Global mean precipitation rate. (d) Kinetic energy extraction time scale. (e) Kinetic energy residence time. . . . . . . . . . . . . . . . . . . . . . . 3

A.2 Vertical integral of kinetic energy extraction (KEE) from climate model simulations with drag added near the surface and throughout the whole atmosphere: (a) SL(5), (b) WA(7.63), (c) WA(5). . . . . . . . . . . . . . . . . . . . . . . . . . . . 6

A.3 Zonally and vertically averaged mean meridional (top) and transient plus stationary eddy (bottom) contributions to the meridional transport of sensible heat, in PW. . . . . . . . . . . 8
A.4 Zonally and vertically averaged mean meridional (top) and transient plus stationary eddy (bottom) contributions to the meridional transport of momentum, in $10^{18}$ kg $m^2s^{-1}$. . . . . . 8
A.5 Spatial variance of temperature on constant pressure surfaces as a function of height for near-surface model runs (left) and whole-atmosphere runs (right). The units are Kelvin squared. 10
A.6 Rate of pressure work done by each pressure level on the atmosphere above. . . . . . . . . . . . . . . . . . . . . . . . . . 11
A.7 Zonally averaged convective and large-scale precipitation for selected surface-only and whole-atmosphere cases. . . . . . . 13